Poisoning of Solid Oxide Electrolysis Cells by Impurities

Ebbesen, Sune; Graves, Christopher R.; Hauch, Anne; Jensen, Søren Højgaard; Mogensen, Mogens Bjerg

Published in:
Journal of The Electrochemical Society

Link to article, DOI:
10.1149/1.3464804

Publication date:
2010

Document Version
Publisher's PDF, also known as Version of record

Journal of The Electrochemical Society, **157** (10) B1419-B1429 (2010)
0013-4651/2010/157(10)/B1419/11/$28.00 © The Electrochemical Society

Poisoning of Solid Oxide Electrolysis Cells by Impurities

Sune D. Ebbesen,[a,z] Christopher Graves,[a,b,*] Anne Hauch,[a] Søren H. Jensen,[a] and Mogens Mogensen[a,]**

[a]*Fuel Cells and Solid State Chemistry Division, Risø National Laboratory for Sustainable Energy, The Technical University of Denmark, 4000 Roskilde, Denmark*
[b]*Lenfest Center for Sustainable Energy and Department of Earth and Environmental Engineering, Columbia University, New York, New York, 10027 USA*

Electrolysis of H_2O, CO_2, and co-electrolysis of H_2O and CO_2 was studied in Ni/yttria-stabilized zirconia (YSZ) electrode supported solid oxide electrolysis cells (SOECs) consisting of a Ni/YSZ support, a Ni/YSZ electrode layer, a YSZ electrolyte, and an lanthanum strontium manganite (LSM)/YSZ oxygen electrode When applying the gases as received, the cells degraded significantly at the Ni/YSZ electrode, whereas only minor (and initial) degradation was observed for either the Ni/YSZ or LSM/YSZ electrode. Application of clean gases to the Ni/YSZ electrode resulted in operation without any long-term degradation, in fact some cells activated slightly. This shows that the durability of these SOECs is heavily influenced by impurities in the inlet gases. Cleaning the inlet gases to the Ni/YSZ electrode may be a solution for operating these Ni/YSZ-based SOECs without long-term degradation.
 [DOI: 10.1149/1.3464804]

Manuscript submitted June 3, 2010; revised manuscript received June 22, 2010. Published August 13, 2010.

The production of synthetic hydrocarbon fuels from renewable energy is a solution to reduce oil consumption and carbon dioxide emissions without the need for modifications of existing infrastructure, e.g., in the production of methane (also called synthetic natural gas) or petrol/diesel, the infrastructure already exists in many countries. The raw material for synthetic hydrocarbon fuels is synthesis gas (H_2 + CO), which traditionally is produced via coal gassification or steam reforming of natural gas. Both processes consume fossil fuels and emit greenhouse gases. Co-electrolysis of H_2O and CO_2 ($H_2O + CO_2 + \text{electricity} \rightarrow H_2 + CO + O_2$) using renewable energy sources may be an alternative route for producing synthesis gas without consumption of fossil fuels and without emitting greenhouse gases. CO_2 capture from air and/or recycling or reuse of CO_2 from energy systems[1-8] in combination with co-electrolysis of H_2O and CO_2 seems to be an attractive method to provide CO_2 neutral synthetic hydrocarbon fuels.[9-11] Solid oxide electrolysis cell (SOECs) have the potential for cost competitive production of hydrogen,[11-14] carbon monoxide,[11] and synthesis gas,[9,15] providing lifetimes exceeding 5–10 years.[11,14]

Steam electrolysis $\left(H_2O + \text{electricity} \rightarrow H_2 + \frac{1}{2}O_2\right)$ in solid oxide cells (SOCs) for hydrogen production was under development during the early 1980s[16-18] and has again become increasingly investigated during recent years as a green energy technology.[11,19,20] Only limited studies have reported electrolysis of CO_2 $\left(CO_2 + \text{electricity} \rightarrow CO + \frac{1}{2}O_2\right)$ in SOCs.[11,17,21-27] Most of this work was performed in platinum and nickel-based SOCs at NASA as a means of producing oxygen.[17,21,22] Co-electrolysis of H_2O and CO_2 is more complicated than the two separate electrolysis reactions because the equilibrium for the water gas shift (WGS)/reverse water gas shift (RWGS) reaction ($CO + H_2O \underset{\text{RWGS}}{\overset{\text{WGS}}{\rightleftarrows}} CO_2 + H_2$) is easily reached over nickel catalysts at the operating temperatures of the SOEC[28] and occurs in parallel with the electrochemical reactions.[15] So far, the co-electrolysis of H_2O and CO_2 has only been presented in a few studies.[15,29-32]

Relatively little information on the long-term stability of Ni/yttria-stabilized zirconia (YSZ)-based SOECs is available. A few studies have reported short-term (shorter than 500 h)[32-35] and long-term (longer than 500 h)[9,15,24,36-44] durability. Even though the initial performance may be quite similar in the electrolysis and fuel cell mode, the cells degrade much faster in the electrolysis mode than in the fuel cell mode.[39,45,46] When operating Ni/YSZ–YSZ–lanthanum strontium manganite (LSM)/YSZ SOECs at mild conditions, the cells have a limited degradation on the LSM/YSZ electrode, whereas the main degradation occurs on the Ni/YSZ cathode.[39,42] One of the most discussed phenomena for Ni/YSZ electrode degradation in general [both solid oxide fuel cell (SOFC) and SOEC] is the influence of impurities.[9,15,24,37,39,47-59] For SOFCs the poisoning effect of sulfur is the most discussed, whereas for SOECs the impurities are rarely identified. The impurities tend to migrate to the grain boundaries, blocking the active triple phase boundary (TPB), which leads to an increase mainly in the polarization resistance. Also for SOECs, the segregation of impurities to the TPB in the Ni/YSZ electrode was speculated to cause the observed degradation when operated at mild conditions (in H_2O, CO_2, or H_2O–CO_2 mixtures),[9,15,24,37,39,49] although no firm evidence for this degradation mechanism for SOECs has been presented. We have recently shown that removing these impurities may result in electrolysis durability with only limited degradation when operated at low current densities.[9,37]

The aim of the present study is to examine the degradation of Ni/YSZ-based SOECs when applied for the electrolysis of H_2O, CO_2, and co-electrolysis of H_2O and CO_2 in detail by electrochemical impedance spectroscopy (EIS) and to investigate the influence of impurities on the performance and durability of the SOECs.

Experimental

Planar Ni/YSZ-supported SOCs of 5 × 5 cm with an active electrode area of 4 × 4 cm were used for all experiments. The cells were produced at Risø DTU[45,60] and had a 10–15 μm thick Ni/YSZ cermet electrode; a 10–15 μm thick YSZ electrolyte and a 15–20 μm thick strontium-doped lanthanum manganate composite LSM/YSZ electrode. The cells were supported by an ~300 μm thick porous Ni/YSZ layer.[60,61] At startup, the nickel oxide in the Ni/YSZ electrode was reduced to nickel in hydrogen at 1000°C.

It was previously published that test components, such as the application of glass sealings,[39] may have a significant negative effect on the long-term stability of these cells. To eliminate the glass sealings, three different cell assemblies were used for characterization of the cells (see Fig. 1). The cell assemblies used for each specific experiment are described in Table I. For all the cell assemblies, the cell was sandwiched between the gas distributor/contact components at each electrode. A gold or platinum foil at the side of the LSM/YSZ electrode and a nickel foil at the side of the Ni/YSZ electrode were used to pick up the electrode current. For cell assembly 1, the test house was assembled using albite glass seals and gas distributor/contact components, which were made of the same material as the respective electrodes.[62] For cell assembly 2 (Fig. 1), the

* Electrochemical Society Student Member.
** Electrochemical Society Active Member.
z E-mail: SUEB@risoe.dtu.dk

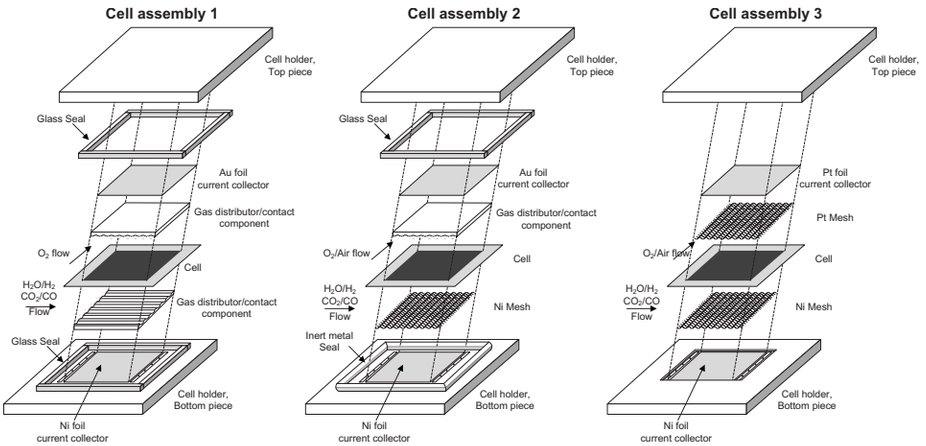

Figure 1. Cell assemblies in a cross-flow pattern. Cell assembly 1 with glass seal and gas distributor/contact component. Cell assembly 2 with metal seal and nickel mesh as gas distributor/contact component at the side of the Ni/YSZ electrode and glass seal and traditional gas distributor/contact component at the side of the LSM/YSZ electrode. Cell assembly 3 without the use of a sealing material and with meshes as gas distributor/contact component at both sides of the cell.

glass seal and gas distributor/contact component on the side of the Ni/YSZ electrode were replaced with a nickel seal and a nickel mesh.[15] External gas leaks were minimized by applying Ni/YSZ paste (to fill any irregularities) at the side of the Ni/YSZ electrode. For cell assembly 3, the gas distributors at both electrodes were replaced with a metal mesh as gas distributor/contact component (nickel mesh on the side of the Ni/YSZ electrode and platinum mesh on the side of the LSM/YSZ electrode).[15] The use of platinum mesh on the side of the LSM/YSZ electrode avoided stresses induced by uneven weight on the two sides of the cell. Further, the use of a sealing material was avoided by lowering the gas distribution/contact component and current collector into a wide channel made in the alumina cell housing. In this case, the cell rests directly on the alumina housing. Gas leaks were minimized by applying Ni/YSZ paste at the side of the Ni/YSZ electrode and platinum paste at the side of the LSM/YSZ electrode. For all assemblies, the metal seals and meshes are assumed to contribute negligible to the electrochemical/catalytic activity because their surface area is low compared to the surface area of the electrodes.

Several voltage probes were drawn through the alumina block to measure the cell voltage and the in-plane voltage. The in-plane voltage is measured across each electrode by probes contacting the electrode near the gas inlet and outlet. The in-plane voltage, which reflects an uneven current distribution, is usually below 1 mV due to the high conductivity of the metal foils applied for current collection. Thus, an in-plane voltage of, say 1 mV, reflects that a significant current flows in-plane through the metal foil due to the uneven current distribution across the cell. The cells were placed in a furnace to operate the SOCs at the desired temperature. Steam was produced by reacting oxygen with hydrogen at the inlet to the alumina cell housing.

To investigate the effect of the impurities in the applied gases, the initial performance and electrolysis durability were examined by (a) applying the gases as received (oxygen: industrial grade, $O_2 \geq 99.5\%$, Air Liquide; hydrogen: N30, $H_2 \geq 99.9\%$, Air Liquide; CO_2: industrial grade, $CO_2 \geq 99{,}7\%$, Air Liquide; and CO: N20, $CO \geq 99.0\%$, Air Liquide) and (b) applying cleaned inlet gases as recently shown for single cell testing[9] and stack testing.[37] The method for cleaning the inlet gases during co-electrolysis[37] and CO_2 electrolysis[9] was extremely effective, and operation without degradation is possible.[9,37] The method for cleaning the inlet gases to both the Ni/YSZ and LSM/YSZ electrodes is currently subject to a pending patent application[63] and will be described in a later publication. For all experiments in which cleaned gases were applied, CO_2, CO, and H_2 was cleaned, and in the co-electrolysis, O_2 was also cleaned (used both for the production of steam and supplied to the LSM/YSZ electrode). Gas analysis by mass spectrometry (OmniStar GSD 301 01) was performed in an attempt to specify the impurities.

Initial electrochemical characterization of the SOCs.— After reduction, the cell was characterized in H_2O–H_2 mixtures following a standard procedure at Risø DTU. This procedure consists of ac and dc characterization in the temperature range from 750 to 850°C with various gas mixtures supplied to the Ni/YSZ electrode (4% H_2O–96% H_2, 20% H_2O–80% H_2, and 50% H_2O–50% H_2) and pure oxygen or air supplied to the LSM/YSZ electrode. For the investigation of CO_2 electrolysis and co-electrolysis of H_2O and CO_2, additional ac and dc characterization was performed with H_2O–CO_2–H_2–CO mixtures supplied to the Ni/YSZ electrode.

The dc characterization of the cell was performed by recording polarization curves [current density–voltage (*i-V*) curves] in both electrolysis and fuel cell mode by varying the current. AC characterization was performed by EIS using an external shunt and a Solartron 1255B or 1260 frequency analyzer at frequencies from 82 kHz to 0.08 Hz. The impedance data were corrected using the short-circuit impedance response of the test setup. From the impedance spectra, the ohmic (serial) resistance (R_s) was taken as the value of the real part of the impedance measured at 82 kHz. The polarization resistance (R_p) was taken as the difference in the real part of the impedance at 82 kHz and 0.08 Hz. The total area specific resistance of a cell was calculated as the total ac resistance of the real part ($R_s + R_p$, to 0.08 Hz) of the impedance measured at open-circuit voltage (OCV).

Durability of the SOECs.— The durability of the SOCs during H_2O and CO_2 electrolysis and co-electrolysis of H_2O and CO_2 was examined for nine identical cells, all operated at 850°C (see Table I). Three experiments were performed with the gases applied as received. The cell voltage histories when applying the gases as received for H_2O electrolysis (50% H_2O–50% H_2, 850°C, -0.50 A/cm^2),[41] CO_2 electrolysis (70% CO_2–30% CO, 850°C, -0.25 A/cm^2),[9,24] and co-electrolysis (45% CO_2–45% H_2O–10% H_2, 850°C, -0.25 A/cm^2)[15] were previously reported. For all tests applying the gases as received, oxygen was supplied to the LSM/YSZ electrode to avoid any transients in the polarization resistance. The specific degradation rates when applying the gases as received were impossible to reproduce, see for example Ref. 15, 24, 39, and 42.

The electrolysis durability was examined with cleaned inlet gases for six identical SOCs at the same conditions as when applying the gases as received. Two cells were tested for CO_2 electrolysis durability at 850°C and a current density of -0.25 A/cm^2 (70% CO_2–30% CO); these cells are denoted as A_{CO_2} and B_{CO_2}. Two cells were tested for H_2O electrolysis durability at 850°C and a current density of either -0.25 A/cm^2 or -0.50 A/cm^2 (50% H_2O–50% H_2); these cells are denoted as A_{H_2O} and B_{H_2O},

respectively. Also, two cells were tested for co-electrolysis durability at 850°C and a current density of −0.25 A/cm^2 (45% H_2O–45% CO_2–10% H_2); these cells are denoted as $A_{H_2O-CO_2}$ and $B_{H_2O-CO_2}$. For these six SOCs except $A_{H_2O-CO_2}$, oxygen was supplied to the LSM/YSZ electrode. For $A_{H_2O-CO_2}$, air was supplied to the LSM/YSZ electrode. The cell voltage history for cell B_{CO_2} was previously reported in a paper.[9] All SOCs except A_{CO_2} and $B_{H_2O-CO_2}$ were tested for electrolysis durability for 600 h. Cells A_{CO_2} and $B_{H_2O-CO_2}$ were operated for only 70 or 520 h, respectively, due to unintended shutdowns.

AC characterization during durability testing.— Electrochemical impedance spectra were recorded during the electrolysis tests to examine the cause of the passivation/degradation. To improve the frequency resolution of the spectra recorded during electrolysis testing, analysis of the difference in impedance spectra (ADIS) was performed.[46] The difference in the impedance was calculated from the real part of the experimental impedance, $Z'(f)$, according to Eq. 1 with $Z'(f)_{t=\text{reference time}}$ used as the reference. The reference time is either the start of electrolysis or the start of passivation, activation, or degradation. The specific reference time is stated in the text

$$\frac{\Delta_t\, \partial\, Z'(f)}{\partial\ \ln(f)} = \frac{[Z'(f_{n+1})_t - Z'(f_{n-1})_t] - [Z'(f_{n+1})_{t=\text{reference time}} - Z'(f_{n-1})_{t=\text{reference time}}]}{\ln(f_{n+1}) - \ln(f_{n-1})} \quad [1]$$

ADIS enables examination of the characteristic frequency for the specific degradation. As previously described for this type of Ni/YSZ-based SOCs produced at Risø DTU, the impedance contributions from each of the two electrodes, can be described by an equivalent circuit consisting of an inductance, an ohmic resistance, and five subcircuits consisting of a resistance in parallel with a constant phase element.[64] When characterizing fresh cells at 850°C with 25% H_2O–75% H_2 supplied to the Ni/YSZ electrode and air to the LSM/YSZ electrode the five RQ subcircuits represent a high frequency LSM/YSZ electrode arc (~50 kHz), a contribution from the TPB reaction in the Ni/YSZ electrode (~8000 Hz), a low frequency LSM electrode arc (~1100 Hz), a gas diffusion arc[65,66] (~20–100 Hz), and a gas conversion arc[43,65,67] (~3 Hz). The contribution from gas diffusion and gas conversion originate mainly from the Ni/YSZ electrode. The resistances and frequencies should only be used as a guideline because variation in performance between the produced cells occur, and slightly different resistances/frequencies are observed when changing the current density and gas compositions, e.g., steam content to the Ni/YSZ electrode and oxygen content to the LSM/YSZ electrode.[64,68] Combining ADIS with the characteristic frequencies observed in the equivalent circuit model, the degradation phenomena can be assigned to a specific electrode and electrode process.

Gas shift analysis by EIS.— Variation in the gas compositions ("gas shifts") supplied to both the Ni/YSZ and LSM/YSZ electrodes was performed for all tests. The impedance measured from the gas shifts, combined with ADIS enables identification of the impedance contributions from each of the two electrodes. Before electrolysis, spectra were recorded at OCV first keeping the gas composition to the Ni/YSZ electrode constant, while spectra were recorded with oxygen or synthetic air to the LSM/YSZ electrode (O_2/N_2 = 21/79). Afterward, the oxygen concentration to the LSM/YSZ electrode was kept constant while recording spectra in various atmospheres at the Ni/YSZ electrode. For CO_2 and co-electrolysis, the shift in gas composition to the Ni/YSZ electrode was from 70% CO_2–30% CO to 50% CO_2–50% CO, whereas for H_2O electrolysis the shift was from 20% H_2O–80% H_2 to 50% H_2O–50% H_2. A similar set of impedance spectra were recorded at OCV after electrolysis.

ADIS of the impedance spectra measured during the gas shifts was performed by subtraction of two spectra where a gas shift was made for one electrode only. The change in impedance is calculated according to Eq. 2-4, where $\partial Z'(f)_{Ni/YSZ}/\partial\ \ln(f)$ for the gas shift in CO_2–CO(II) or in H_2O–H_2(III) at the Ni/YSZ electrode or the shift in O_2–N_2(IV) at the LSM/YSZ electrode is shown

$$\frac{\partial\, Z'(f)_{Ni/YSZ}}{\partial\ \ln(f)} = \frac{Z'(f)_{50\%\ CO_2-50\%\ CO} - Z'(f)_{70\%\ CO_2-30\%\ CO}}{\partial\ \ln(f)} \quad [2]$$

$$\frac{\partial\, Z'(f)_{Ni/YSZ}}{\partial\ \ln(f)} = \frac{Z'(f)_{20\%\ H_2O-80\%\ H_2} - Z'(f)_{50\%\ H_2O-50\%\ H_2}}{\partial\ \ln(f)} \quad [3]$$

$$\frac{\partial\, Z'(f)_{LSM/YSZ}}{\partial\ \ln(f)} = \frac{Z'(f)_{100\%\ O_2} - Z'(f)_{21\%\ O_2-79\%\ N_2}}{\partial\ \ln(f)} \quad [4]$$

The difference in the gas shift before and after durability tests for the Ni/YSZ or the LSM/YSZ electrode is calculated, as shown below, where $\Delta_{\text{gas shift}}(\partial Z'(f)_{Ni/YSZ}/\partial\ \ln(f))$ for the gas shift at the Ni/YSZ electrode and $\Delta_{\text{gas shift}}(\partial Z'(f)_{LSM/YSZ}/\partial\ \ln(f))$ for the gas shift at the LSM/YSZ electrode is shown in Eq. 5 and 6, respectively

$$\Delta_{\text{gas shift}}\frac{\partial\, Z'(f)_{Ni/YSZ}}{\partial\ \ln(f)} = \frac{\partial\, Z'(f)_{Ni/YSZ,\ \text{after electrolysis}}}{\partial\ \ln(f)} - \frac{\partial\, Z'(f)_{Ni/YSZ,\ \text{before electrolysis}}}{\partial\ \ln(f)} \quad [5]$$

$$\Delta_{\text{gas shift}}\frac{\partial\, Z'(f)_{LSM/YSZ}}{\partial\ \ln(f)} = \frac{\partial\, Z'(f)_{LSM/YSZ,\ \text{after electrolysis}}}{\partial\ \ln(f)} - \frac{\partial\, Z'(f)_{LSM/YSZ,\ \text{before electrolysis}}}{\partial\ \ln(f)} \quad [6]$$

Results

Initial electrochemical characterization of the SOCs.— The results of this initial ac characterization for the nine cells are summarized in Table I. Some variation in the ohmic resistances is observed, whereas the polarization resistances for the nine cells were reproducible in the different gas mixtures. The variation in the ohmic resistance was mainly a consequence of variations in the contact between the current collector, gas distribution component, and the cell. In general, for the cells using assemblies 2 and 3, good contact was ensured, which clearly improved the reproducibility.

Durability of the SOECs when applying gases as received.— Cell voltage and in-plane voltage during CO_2 electrolysis.— After testing the initial performance of the cell, durability in electrolysis mode was examined at 850°C with 70% CO_2–30% CO supplied to the Ni/YSZ electrode and a current density of −0.25 A/cm^2. The evolution of the cell voltage and in-plane voltage with time for the test is shown in Fig. 2A.

During the initial electrolysis period (50 h), the cell voltage increased slightly, corresponding to a passivation rate of 0.217 mV/h. The loss in cell performance during CO_2 electrolysis was at least partly reversible when introducing hydrogen;[24] the term passivation is therefore used to describe the loss in performance. Hereafter, the passivation rate increased to 0.454 mV/h (passivation rate from 300 to 400 h). After operation for ~500 h the cell voltage leveled off, and the cell voltage reached a plateau with a limited passivation rate of only 0.032 mV/h.

The in-plane voltage for the Ni/YSZ electrode (Fig. 2A) increased corresponding to the increase in cell voltage. After operation for ~100 h, the in-plane voltage leveled off. Subsequently, the in-plane voltage decreased to the same value as when the electrolysis period was started. During the long-term passivation where the cell voltage increased only slightly, the in-plane voltage remained close to stable.

Cell voltage and in-plane voltage during H_2O electrolysis.— Electrolysis durability was tested at 850°C with 50% H_2O–50% H_2

Table I. Cell assembly and initial characterization of the nine SOCs. Area-specific polarization resistances calculated from EIS for the cells when characterized in 20% H_2O–80% H_2, 50% H_2O–50% H_2, 50% CO_2–50% CO, 70% CO_2–30% CO, and 45% CO_2–45% H_2O–10% H_2 at OCV and 850°C.

		Area-specific polarization Resistances measured by EIS at OCV (Ω cm^2)								
		Cells used for H_2O electrolysis			Cells used for CO_2 electrolysis			Cell used for co-electrolysis		
		Gases as received Cell assembly 1	Clean inlet gases Cell assembly 2		Gases as received Cell assembly 1	Clean inlet gases Cell assembly 1		Gases as received Cell assembly 2	Clean inlet gases Cell assembly 3	
Gas composition to the Ni/YSZ electrode	Gas composition to the LSM/YSZ electrode	(R_s = 0.19 [a])	Cell A_{H_2O} (R_s = 0.08)	Cell B_{H_2O} (R_s = 0.09)	(R_s = 0.13 [a])	Cell A_{CO_2} (R_s = 0.08)	Cell B_{CO_2} (R_s = 0.08)	(R_s = 0.09)	Cell $A_{H_2O-CO_2}$ [b] (R_s = 0.12)	Cell $B_{H_2O-CO_2}$ [b] (R_s = 0.08)
20% H_2O–80% H_2	Air	0.21	0.19	0.19		0.18	0.19	0.19	0.19	0.18
	Oxygen	0.18	0.15	0.15		0.15	0.16	0.14	0.16	0.15
50% H_2O–50% H_2	Air		0.15	0.15	0.14	0.13	0.15	0.15	0.15	0.14
	Oxygen	0.13	0.11	0.12	0.11	0.10	0.12	0.10	0.12	0.10
50% CO_2–50% CO	Air				0.21	0.18	0.20	0.20	0.21	0.21
	Oxygen				0.17	0.15	0.17	0.15	0.17	0.16
70% CO_2–30% CO	Air				0.24	0.20	0.23	0.22	0.23	0.23
	Oxygen				0.19	0.17	0.19	0.17	0.20	0.19
45% CO_2–45% H_2O–10% H_2 [c]	Air								0.23	0.23
	Oxygen							0.24	0.21	0.20

[a] The increased ohmic resistance for these experiments is most likely caused by nonoptimal contact between the current collector, contact components, and the cell (as have been the experience with cell assembly 1, Fig. 1).

[b] The increased resistance for cell $A_{H_2O-CO_2}$ compared to the remaining experiment was mainly observed in R_S. This increase in resistance is most likely due to the small amount of contact points between the contact component (mesh) and the LSM/YSZ electrode for this experiment. When increasing the amount of contact points at the LSM/YSZ electrode ($B_{H_2O-CO_2}$) more predictable ohmic resistance was obtained.

[c] We have previously shown that the gas composition to the Ni/YSZ electrode is in WGS–RWGS equilibrium.[15] The thermodynamic equilibrium composition for the co-electrolysis mixture is 40% CO_2, 50% H_2O, 5% CO, 5% H_2 at 850°C.

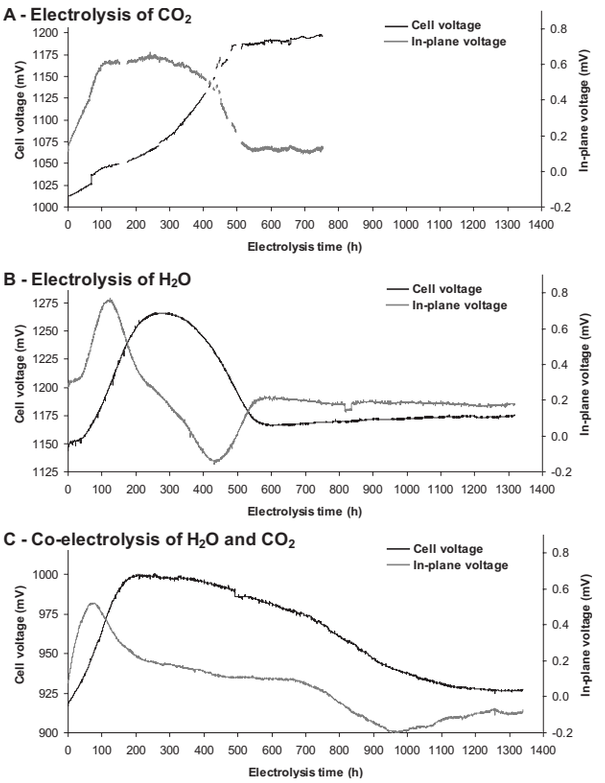

Figure 2. Cell voltage and corresponding in-plane voltage at the Ni/YSZ electrode measured during (A) CO_2 (850°C, −0.25 A/cm^2, 70% CO_2–30% CO), (B) H_2O (850°C, −0.50 A/cm^2, 50% H_2O–50% H_2), and (C) co-electrolysis (850°C, −0.25 A/cm^2, 45% H_2O–45% CO_2–10% H_2).

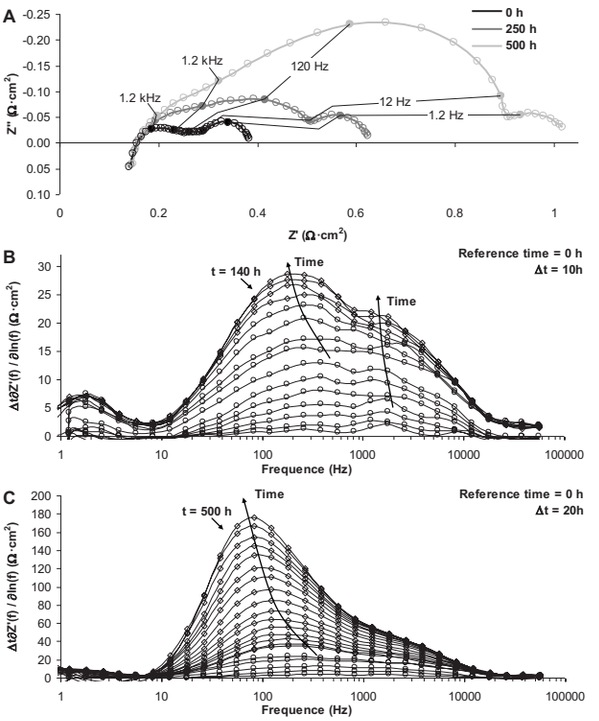

Figure 3. (A) Nyquist plot of impedance spectra recorded during CO_2 electrolysis. ADIS (B) during the initial passivation of the cell (0–140 h) and (C) during the entire passivation period (0–500 h).

supplied to the Ni/YSZ electrode and a current density of −0.50 A/cm^2. The evolution of cell voltage and in-plane voltage with time for the test is shown in Fig. 2B.

During the initial electrolysis period, the cell voltage increased slightly, corresponding to a passivation rate of 0.080 mV/h during the first 50 h of operation. Hereafter, the passivation rate increased to 0.683 mV/h (passivation rate from 100 to 200 h). After operation for ~250 h the cell voltage started to level off, where after it decreased again (activation). The activation rate measured from 400 to 500 h of operation was 0.497 mV/h. After activation of the cell, a long-term degradation rate of 0.015 mV/h was observed (700–1100 h).

The in-plane voltage for the Ni/YSZ electrode (Fig. 2B) follows the first derivative of cell voltage with time. After operation for ~125 h the in-plane voltage levels off. Subsequently, the in-plane voltage decrease to the same value as when the electrolysis period was started. During activation a decrease to a negative in-plane voltage occurs. During the long-term degradation where the cell voltage increased only slightly, the in-plane voltage remained close to stable.

Cell voltage and in-plane voltage during co-electrolysis of H_2O and CO_2.— After testing the initial performance of the cell, durability in electrolysis mode was tested at 850°C with 45% H_2O–45% CO_2–10% H_2 supplied to the Ni/YSZ electrode and a current density of −0.25 A/cm^2. The thermodynamic equilibrium composition for the co-electrolysis mixture is 50% H_2O –40% CO_2–5% CO–5% H_2 at 850°C.[69] The evolution of the cell voltage and in-plane voltage with time for the entire test is shown in Fig. 2C.

The cell voltage during co-electrolysis shows the same trend (passivation/activation) as during H_2O electrolysis (Fig. 2B), although the initial period with low passivation is not as pronounced. The initial (50 h) passivation rate during co-electrolysis was 0.377 mV/h. Hereafter, the passivation rate increased to 0.594 mV/h (passivation rate from 100 to 150 h). After operation for ~200 h, the cell voltage started to level off, whereafter it decreased again. The activation may be separated into two periods; first a period with a low activation rate of 0.067 mV/h (activation rate from 400 to 600 h) followed by a period with an increased activation of 0.138 mV/h (activation rate from 700 to 900 h). After the activation of the cell, a long-term degradation of 0.003 mV/h was observed during the last 50 h of operation.

Also the in-plane voltage for the Ni/YSZ electrode shows the same trend as during H_2O electrolysis (Fig. 2B). The in-plane voltage increases initially. After operation for ~75 h the in-plane voltage levels off. Subsequently, the in-plane voltage decreases to the same value as when the electrolysis period was started. During the initial activation, the in-plane voltage remained close to stable, whereas during the fast activation, a decrease to a negative in-plane voltage occurs. During the long-term degradation where the cell voltage increased only slightly, the in-plane voltage remained close to stable.

EIS during electrolysis applying gases as received.— Significant degradation of the SOECs was observed when applying the inlet gases as received. To investigate the origin for the degradation, impedance spectra were recorded during electrolysis, as shown below.

Electrolysis of CO_2. Nyquist plot of the measured impedance during CO_2 electrolysis as well as ADIS ($\Delta_t\, \partial\, Z'(f)/\partial\, \ln(f)$) during electrolysis are shown in Fig. 3. Figure 3A shows that no change is observed in the ohmic resistance during electrolysis testing and that the observed cell degradation is caused solely by a change in the polarization resistance of the cell. The start of electrolysis is used as the reference time for the ADIS shown in Fig. 3. The differences in impedance spectra recorded during CO_2 electrolysis show initial increases at ~200 to 300 Hz (initially close to 1000 Hz) and at ~2000 Hz (Fig. 3B). After electrolysis for ~100 h, the increase in

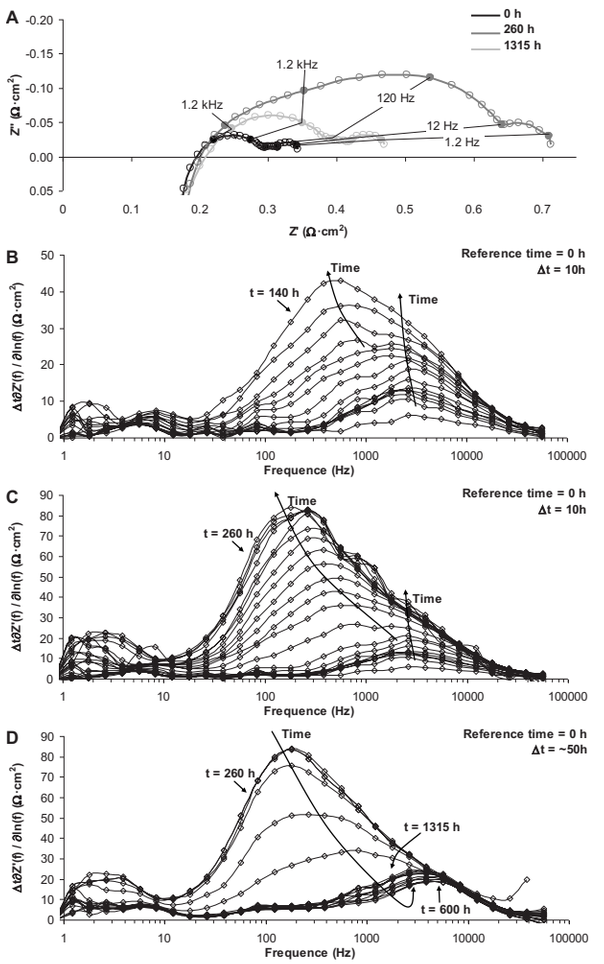

Figure 4. (A) Nyquist plot of impedance spectra recorded during H_2O electrolysis. ADIS (B) during the initial passivation of the cell (0–140 h), (C) during the entire passivation period (0–260 h), and (D) during activation and long-term degradation of the cell (260–1315 h).

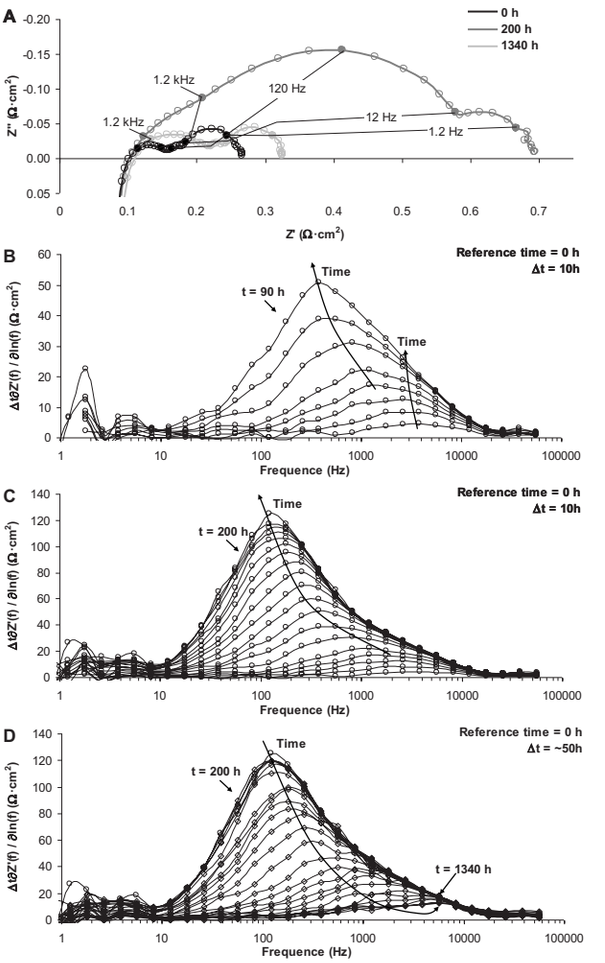

Figure 5. (A) Nyquist plot of impedance spectra recorded during H_2O electrolysis. ADIS (B) during the initial passivation of the cell (0–80 h), (C) during the entire passivation period (0–200 h), and (D) during activation and long-term degradation of the cell (200–1340 h).

the peak at ~2000 Hz leveled off (Fig. 3B), whereas a continued increase in impedance was observed at ~300 Hz, which shifted to ~80 Hz with time (Fig. 3C).

Electrolysis of H_2O. The Nyquist plot of the measured impedance during H_2O electrolysis as well as ADIS ($\Delta_t\, \partial\, Z'(f)/\partial\, \ln(f)$) during electrolysis is shown in Fig. 4. Figure 4A shows that no change is observed in the ohmic resistance during electrolysis testing, whereas the observed cell degradation is caused solely by a change in the polarization resistance of the cell. The start of electrolysis is used as the reference time for the ADIS shown in Fig. 4. During the initial passivation of the cell (0–0 h, Fig. 2), an increase in impedance is observed at around 300–400 (initially close to 1000 Hz) and ~2000 to 3000 Hz (Fig. 4B). After electrolysis for ~50 to 100 h, the increase at ~2000 to 3000 Hz leveled off, whereas a continued increase in impedance was observed at ~600 to 700 Hz (Fig. 4B), which shifted to ~150 to 200 Hz with time (Fig. 4C).

During activation of the cell (250–600 h, Fig. 2), the impedance peak observed at ~150 to 200 Hz decreased, whereas the peak at ~2000 to 3000 Hz remained stable or increased only slightly (Fig. 4D). After activation, an increase in impedance (compared to the start of electrolysis) was observed at ~2000 to 3000 Hz similar to the initial loss in performance. After 600 h of operation (long-term degradation, 600–1315 h, Fig. 2), an increase in impedance is only observed between ~4000 and 5000 Hz (Fig. 4D).

Co-electrolysis of H_2O and CO_2. The Nyquist plot of the measured impedance during co-electrolysis of H_2O and CO_2 as well as ADIS ($\Delta_t\, \partial\, Z'(f)/\partial\, \ln(f)$) during electrolysis is shown in Fig. 5. Figure 5A shows again that no change is observed in the ohmic resistance during electrolysis testing, whereas the observed cell degradation is caused solely by a change in the polarization resistance of the cell. The start of electrolysis is used as the reference time for the ADIS shown in Fig. 5. During the initial passivation of the cell (0–50 h, Fig. 2), an increased impedance is observed at around 300–400 (initially close to 1000 Hz) and ~2000 to 3000 Hz (Fig. 5B). After electrolysis for ~50 to 100 h, the increase at ~2000 to 3000 Hz leveled off (Fig. 5B), whereas a continued increase in the impedance was observed at ~600 to 700 Hz (Fig. 5B), which shifted to ~100 Hz with time (Fig. 5C).

During activation of the cell (200–1200 h, Fig. 2), the impedance observed at ~100 Hz decreased, whereas the peak at ~2000 to 3000 Hz remained stable (Fig. 5D). After activation, an increase in impedance (compared to the start of electrolysis) was observed at ~2000 to 4000 Hz similar to the initial loss of performance.

Gas shift analysis by EIS.— Gas shifts on both the Ni/YSZ and LSM/YSZ electrodes were performed before and after electrolysis testing for all tests. The gas shifts enable breakdown of the imped-

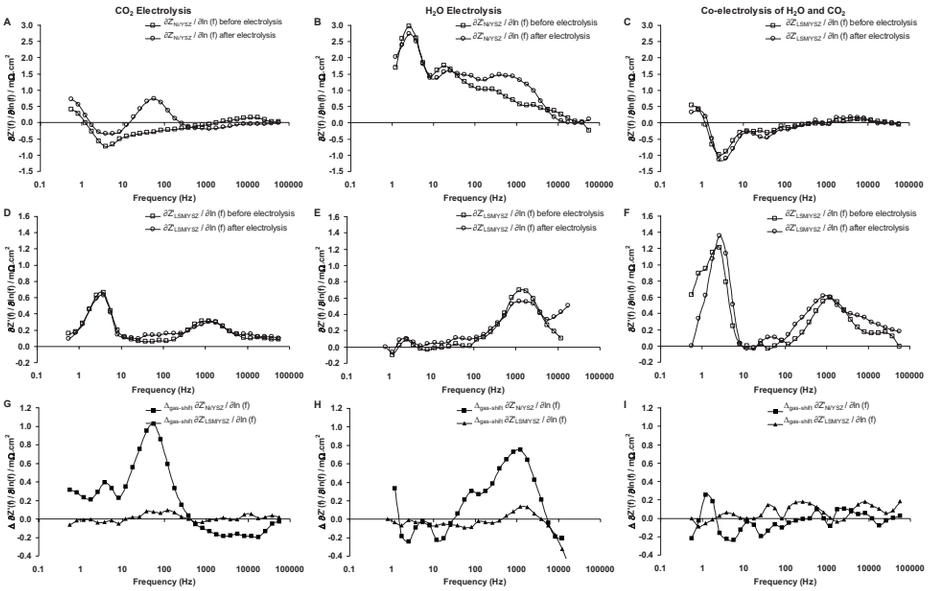

Figure 6. Gas-shift analysis for the three electrolysis test, applying gases as received. [(A)-(C)] Difference in impedance when changing the gas composition to the Ni/YSZ electrode ($\partial Z'(f)_{Ni/YSZ}/\partial\ \ln(f)$), while pure oxygen was supplied to the LSM/YSZ electrode before and after electrolysis. [(D)-(F)] Difference in impedance when changing the gas composition for the LSM/YSZ electrode ($\partial Z'(f)_{LSM/YSZ}/\partial\ \ln(f)$) from pure oxygen to synthetic air while keeping the gas composition to the Ni/YSZ electrode constant. [(G)-(I)] Difference in the gas shift for either the Ni/YSZ or the LSM/YSZ electrode ($\Delta_{gas\ shift}(\partial Z'(f)/\partial\ \ln(f))$). The shift in gas composition for the Ni/YSZ electrode was in CO_2–CO mixtures when applied for CO_2 electrolysis or co-electrolysis of CO_2 and H_2O; for the cell applied for H_2O electrolysis, the shift was in H_2O–H_2 mixtures.

ance contributions from each of the two electrodes and thereby enable assignment of the degradation to a specific electrode or to both electrodes (Fig. 6).

When performing ADIS on the gas shift for the cells applied for H_2O and CO_2 electrolysis (Fig. 6G and H), a significant change in $\partial Z'(f)$ is found for the Ni/YSZ electrode ($\Delta_{gas\ shift}(\partial Z'(f)_{Ni/YSZ}/\partial\ \ln(f))$) whereas only minor changes were observed for the LSM/YSZ electrode ($\Delta_{gas\ shift}(\partial Z'(f)_{LSM/YSZ}/\partial\ \ln(f))$) (Fig. 6G and H). This shows that the main passivation occurs at the Ni/YSZ electrode. The main difference observed for the Ni/YSZ electrode occurs at frequencies ~80 Hz (for CO_2 electrolysis, Fig. 6A and G) and ~100 to 1000 Hz (for H_2O electrolysis, Fig. 6B and H). Because of the low total passivation/degradation of the cell applied for co-electrolysis, no changes in ($\partial Z'(f)/\partial\ \ln(f)$) were observed (Fig. 6). The total degradation of the cell was only 6 mV during the 1350 h.

Durability of the SOECs when cleaning the inlet gases.— Cell voltage and in-plane voltage.— To test the effect of impurities in the inlet gases, experiments with cleaned inlet gases were performed. The durability during electrolysis when applying cleaned inlet gases was examined for six cells at identical electrolysis conditions as the tests shown above (Fig. 2). The evolution of cell voltage and the corresponding in-plane (for two selected cells) with time for the six tests are shown in Fig. 7. Artificial air (as received) was passed over the LSM/YSZ electrode when testing the durability for cell $A_{H_2O–CO_2}$ (45% CO_2–45% H_2O–10% H_2, 850°C, −0.25 A/cm^2), whereas oxygen was supplied to the LSM/YSZ electrode for the remaining cells.

From the cell voltage measured during H_2O electrolysis, CO_2 electrolysis, and co-electrolysis of CO_2 and H_2O (Fig. 7), the degradation was close to zero for A_{CO_2}, B_{CO_2}, and $A_{H_2O–CO_2}$, whereas surprisingly, a minor activation occurred during electrolysis of H_2O (A_{H_2O} and B_{H_2O}) and co-electrolysis of H_2O and CO_2 when supplying oxygen to the LSM/YSZ electrode ($B_{H_2O–CO_2}$).

The cell voltage during CO_2 electrolysis increased slightly during the initial 20 h of operation (cell A_{CO_2}: from 973 to 975 mV and cell B_{CO_2}: from 977 to 980 mV). Thereafter no degradation was observed during the remaining electrolysis period. The cell voltage after 70 h of operation was 974 mV for cell A_{CO_2} and the cell voltage after 600 h of operation was 980 mV for cell B_{CO_2}. The spikes in cell voltage for cell B_{CO_2} at 295 and 363 h of electrolysis operation were caused by a sensor break in the oven temperature control, causing a lowering of the cell temperature to 795 and 835°C, respectively. Also the corresponding in-plane voltage for cell B_{CO_2} shows no change during the electrolysis operation.

Also the cell voltage during H_2O electrolysis increased during the initial electrolysis period. For cell A_{H_2O} (operated at −0.25 A/cm^2), the cell voltage increased slowly from 1014 to 1018 mV (during the first 250 h of electrolysis operation). Hereafter, the

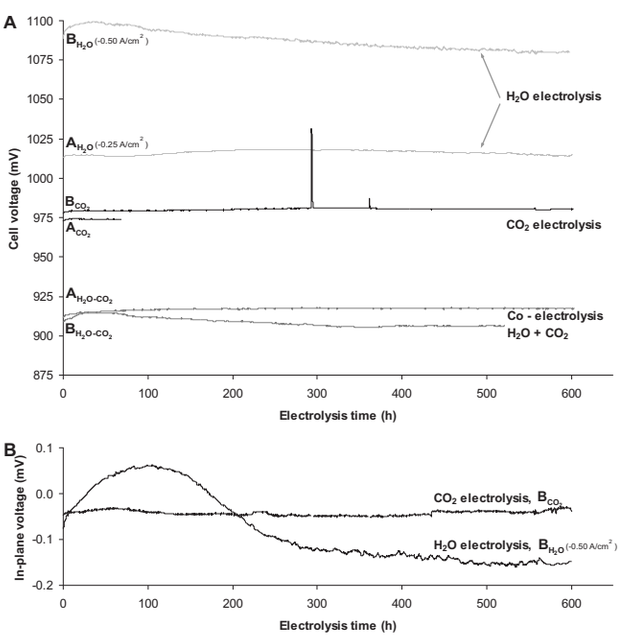

Figure 7. (A) Cell voltage measured during CO_2 electrolysis (850°C, −0.25 A/cm^2, 70% CO_2–30% CO), H_2O electrolysis (850°C, −0.25 A/cm^2 and −0.50 A/cm^2, 50% H_2O–50% H_2), and during co-electrolysis of CO_2 and H_2O (850°C, −0.25 A/cm^2, 45% CO_2–45% H_2O–10% H_2) with cleaned inlet gases. The increase in cell voltage during CO_2 electrolysis after 295 and 363 h of operation was caused by a sensor break in the oven temperature control causing a lowering of the cell temperature to 795 and 835°C, respectively. (B) Corresponding in-plane voltage at the Ni/YSZ electrode measured during either H_2O electrolysis (B_{H_2O}) or CO_2 electrolysis B_{CO_2}.

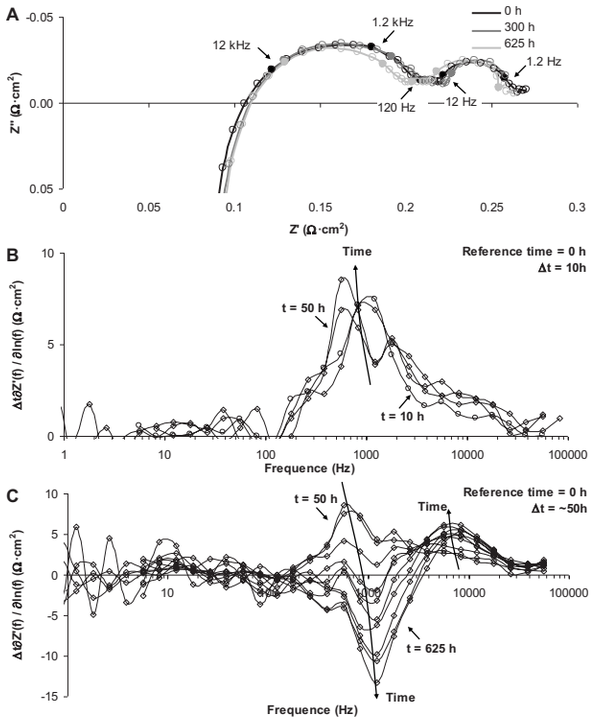

Figure 8. (A) Nyquist plot of impedance spectra recorded during H_2O electrolysis at 850 C, −0.50 A/cm^2, using cleaned gases. ADIS (B) during the initial passivation of the cell (0–50 h) and (C) during the activation of the cell (50–625 h).

cell voltage decreased to the initial value of 1014 mV after 600 h of operation. During the initial 50 h of electrolysis operation, the cell voltage increased from 1089 to 1100 mV for cell B_{H_2O} (operated at −0.50 A/cm^2). Hereafter, the cell voltage decreased to 1080 mV after 575 h of operation. No activation/degradation was observed during the last 55 h of electrolysis operation. The in-plane voltage for cell B_{H_2O} increases initially; after operation for ~100 h the in-plane voltage levels off and subsequently decreases.

The cell voltage during co-electrolysis of CO_2 and H_2O also increased during the initial electrolysis operation. During the first 150 h of electrolysis operation, the cell voltage increased from 912 to 917 mV for cell $A_{H_2O-CO_2}$ (operated with air to the LSM/YSZ electrode). After the first 150 h of operation, no degradation was observed; the cell voltage after 600 h of operation was 917 mV. The initial increase in cell voltage for cell $B_{H_2O-CO_2}$ (operated with oxygen to the LSM/YSZ electrode) occurred during the first 25 h only (the cell voltage increased from 909 to 914 mV). Similar to the cells operated in 50% H_2O–50% H_2, the cell voltage decreased after this initial period. After the first 25 h of operation, the cell voltage decreased to 906 mV after 350 h of operation. During the remaining test period, no change in cell voltage was observed; the cell voltage after the 520 h of operation was 906 mV.

EIS during electrolysis when cleaning the inlet gases.— When cleaning the inlet gases, notable passivation/activation was only observed for cell B_{H_2O}, tested for H_2O electrolysis durability at −0.50 A/cm^2 (Fig. 7). Consequently, the impedance analysis for the experiments using cleaned gases is only shown for cell B_{H_2O}. The Nyquist plot of the measured impedance as well as ADIS ($\Delta_t\, \partial\, Z'(f)/\partial\, \ln(f)$) during electrolysis of H_2O is shown in Fig. 8. The start of electrolysis is used as the reference time for the ADIS shown in Fig. 8.

During the initial passivation of the cell, an increased impedance is observed at ~1000 Hz only (Fig. 8B). During the initial passivation for the remaining cells (both electrolysis of H_2O, CO_2, and co-electrolysis of H_2O and CO_2), an increase in impedance at ~1000 Hz was also observed (not shown), although because of the low passivation/degradation, this increase was not as pronounced.

During the activation of the cell (after electrolysis operation for 50 h), the impedance peak observed at ~1000 Hz decreased, whereas the impedance at 5000–8000 Hz increased (Fig. 8C). The increased peak at 5000–8000 Hz leveled of after around 200 h, whereafter it increased only little (Fig. 8C).

Discussion

Initial performance.— Some variation in the ohmic resistances is observed, whereas the polarization resistances for the nine cells were reproducible in the different gas mixtures. The variation in the ohmic resistance was mainly a consequence of variations in the contact between the current collector, gas distribution component, and the cell. In general, for the cells using assemblies 2 and 3, good contact was ensured, which clearly improved the reproducibility. The varying ohmic resistances may induce increased local current densities (because of uneven contact), which if large enough may induce ohmic degradation (as the local current density is increased to a level where ohmic degradation may occur[70]). No ohmic degradation was observed for any of the current test, showing that the variation in the ohmic resistances did not lead to any degradation.

Cell voltage degradation.— A long-term degradation for the SOECs during electrolysis was observed by the course of the cell voltage (Fig. 2) and the increase in impedance (Fig. 3-5) for the three tests applying the gases as received. As described above, small variations in the initial ohmic resistances was observed, whereas the polarization resistances for the nine cells were reproducible. Consequently, the degradation of the cells, which shows as degradation in the polarization resistance only, is solely a consequence of the operating conditions and not caused by different initial performances.

From the cell voltage shown in Fig. 2, there is a long-term passivation rate between 0.454 and 0.683 mV/h, regardless of the electrolysis conditions. The specific degradation rates when applying the gases as received are difficult to reproduce.[15,24,39,42] However, this study clearly shows that degradation rates can be reproduced and that no degradation occurs when applying cleaned inlet gases. In other words, the durability of these SOCs is heavily influenced by impurities in the inlet gases when operated in electrolysis mode.

Evaluation of the degradation processes by gas shift analysis.— When performing ADIS on the gas shift at OCV (Fig. 6), a significant change in $\partial Z'(f)$ was found for the Ni/YSZ electrode ($\partial Z'(f)_{Ni/YSZ}/\partial\ \ln(f)$), whereas only minor changes were observed for the LSM/YSZ electrode ($\partial Z'(f)_{LSM/YSZ}/\partial\ \ln(f)$) (Fig. 6). This shows that the main passivation occurs at the Ni/YSZ electrode.

Evaluation of the degradation by the course of the in-plane voltage.— The in-plane voltage for the Ni/YSZ electrode (shown in Fig. 2) indicates that the cell passivation may be a transient phenomenon as has previously been reported for passivation/activation during H_2O or CO_2 electrolysis in SOECs[24,42,43] and during sulfur poisoning of SOFCs.[58] The deposition of impurities on specific sites would create such a transient effect by a redistribution of the current as the cell resistance would be lower, where no impurities are deposited as illustrated in Fig. 9. Deposition of impurities, first at the inlet, would create a voltage difference along the flow direction. Because of the increasing passivated area, the in-plane voltage would increase until half of the cell is passivated. At this point, the passivated area is equal to the nonpassivated area and the maximal in-plane voltage would be observed. Likewise, when more than half of the cell is passivated, the in-plane voltage would start to decrease. Finally when the cell is fully passivated, no redistribution of the current takes place and the in-plane voltage would thus be identical to the

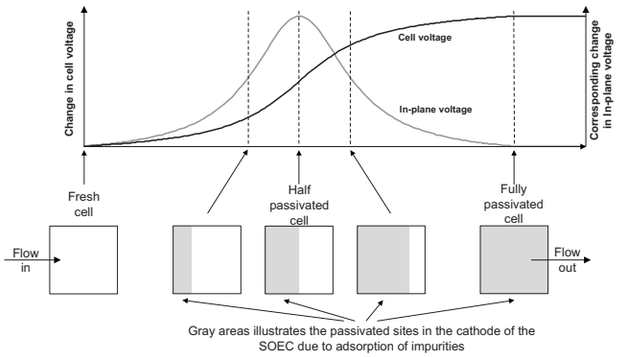

Figure 9. Illustration of the evolution in in-plane and cell voltage due to passivation by adsorption of impurities (the impurities are illustrated by the gray area in bottom sketch) on nickel sites in the cathode of the SOEC after.[24]

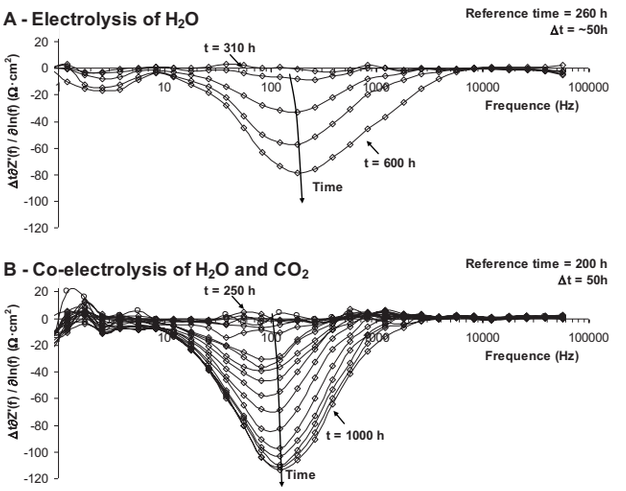

Figure 10. ADIS during activation of the cells for H_2O and co-electrolysis using the spectrum taken when the cell was maximal passivated as reference. (A) ADIS during activation for H_2O electrolysis, the spectrum recorded after 260 h of operation was used as reference. (B) ADIS during activation for co-electrolysis, the spectrum recorded after 200 h of operation was used as reference.

initial in-plane voltage. During activation (by the removal or rearrangement of impurities), a similar in-plane voltage development, although with negative sign, would occur.

Degradation mechanism.— The evolution of cell voltage and in-plane voltage as well as the gas shift analysis when applying the inlet gases as received, indicates that the degradation/passivation is related to adsorption of impurities at active sites in the Ni/YSZ electrode as illustrated in Fig. 9. Because of the extreme low impurity concentration and the impurities adsorb in the anode support layer first, and thereafter in the active anode layer, initially a low passivation rate is observed followed by an increased passivation rate. This agrees with the hypothesis that the degradation is due to impurities, as previously proposed by our group.[9,15,19,24,37,38,40,41,43,49] The impurities may originate from the inlet gases[15,24] or may originate from the test setup, e.g., Si species originating from the glass seal used in assembly 1. In our prior work, the Si-containing impurities were observed to accumulate at TPB boundaries in the Ni/YSZ electrode (determined postmortem by scanning electron microscopy).[40,41,49] The passivation/activation phenomenon was a consequence of these silica impurities. A similar passivation/activation phenomenon was observed during co-electrolysis of H_2O and CO_2 (Fig. 2, 4, and 5), when operated without the use of a glass sealing, and no silica could be detected by postmortem of the cell in this study. Consequently, silica segregation from the glass sealing can certainly not alone describe the observed passivation/activation phenomena during electrolysis. Cleaning the inlet gases (CO_2, CO, and H_2) completely eliminates the observed degradation and almost eliminates the passivation. Therefore, the observed passivation/activation phenomenon is caused by the adsorption of impurities from the inlet gases. As previously discussed, the presence of minute concentrations of sulfur in carbon dioxide, carbon monoxide, and hydrogen in the inlet gases may lead to the observed passivation.[15,24] Traces of hydrogen sulfide (H_2S) were detected by mass spectroscopy in all the gases as supplied in this study, whereas no sulfur could be detected in the cleaned gases. The amount of impurities is in the ppb level,[24] which makes detection extremely difficult.

When applying clean gases, a long-term activation is observed only when water is present. This indicates that water influences the long-term activation. It may be speculated that impurities [e.g., Na (133 ppm), Si (33 ppm), or Al (26 ppm)[40]] in the raw materials may be removed as hydroxides as previously suggested for silica species[40] thereby freeing active sites and improving the activity.

It may further be speculated that the presence of sodium or alumina migrating from the raw material to the surface, as determined for YSZ[50] (and eventually to the gas phase), result in the activation when applying the gases as received (Fig. 2), as especially sodium may bind sulfur as NaHS or Na_2S thereby capturing/removing sulfur from the active sites. Pretreatment of the cell (e.g., with steam) to force these "impurities" to the surface may be a possibility to decrease the degradation, although this probably only has a limited effect as the impurities are "saturated"/covered eventually. Another possibility for the activation is that the glassy phase that block the TPB may crystallize, which has a less blocking effect at the TPB. In this case, steam would decrease the viscosity of the glass, which increases the crystallization kinetics.

Even though the initial performance is similar in electrolysis and fuel cell mode, the cells degrade much faster in electrolysis mode compared to fuel cell mode, where no degradation was observed for identical SOFCs operated at a current density of 0.25 A/cm^2,[45] when applying gases of the same purity.[71] For H_2O electrolysis, CO_2 electrolysis, and co-electrolysis, the volume flow toward the TPB is higher than the volume flow away from the TPB. Further, steam is a good solvent/"evaporator" that during H_2O electrolysis and co-electrolysis gets reduced to H_2 at the TPB creating a transport gradient toward the TPB. This indicates that the driving force of the impurities would be toward the TPB in electrolysis mode. Likewise, in fuel cell mode, the volume flow and water gradient, and thereby the driving force for the impurities would be away from the TPB. Consequently, when operating the SOCs as electrolysis cells, the effect of impurities may be more pronounced compared to operation in fuel cell mode.

Degradation mechanism monitored by EIS.— Careful examination of the evolution in impedance during the passivation/degradation of the SOECs, performed by ADIS (Fig. 4), shows that the same two passivation/degradation processes occur during electrolysis of CO_2, H_2O, and co-electrolysis of CO_2 and H_2O when applying the inlet gases as received. One degradation process is characterized by a characteristic frequency at ~1000 to 3000 Hz (initial degradation). A second passivation phenomenon occurs at a characteristic frequency at ~100 to 200 Hz.

Passivation characterized by a frequency of 100–200 Hz.— Based on the characteristic frequency and the gas shift analysis (Fig. 6), the passivation phenomena (100–200 Hz) may be assigned to a degradation of the Ni/YSZ electrode.

Figure 10 shows the ADIS ($\Delta_t\, \partial\, Z'(f)/\partial\, \ln(f)$) during activation for H_2O electrolysis and co-electrolysis of H_2O and CO_2. The activation of the cell is mainly influenced by the process characterized by the frequency at 100–200 Hz (Fig. 10). The start of the activation

period (260 and 200 h for H_2O and co-electrolysis, respectively) is used as the reference time for the ADIS shown in Fig. 10. That the activation is influenced by a process characterized by the frequency at 100–200 Hz strongly suggests that it is the same process that is affected both during the passivation and the following activation of the electrolysis cell.

It was previously discussed that one single process occurred during the degradation/passivation and activation of the cell and that this single process was characterized by a frequency shifting down from 2000 Hz to ~100 to 200 Hz during the passivation and shifting back to 2000 Hz during activation.[39] Nevertheless, the carefully performed ADIS, as shown in this study, shows that two processes occur: one process that passivates and may activate again (100–200 Hz) and the other process which only shows degradation (1000–3000 Hz) (Fig. 4).

When a clean system is studied, e.g., by using cell assemblies 2 or 3 and cleaned inlet gases, the passivation/degradation of the Ni/YSZ electrode, with a characteristic frequency of 100–200 Hz can be fully eliminated, showing that this process is related to adsorption of impurities at the TPB. The characteristic frequency of 100–200 Hz may be assigned to a partial blockage of the TPB in the Ni/YSZ electrode caused by adsorption of impurities.

Initial degradation characterized by a frequency of 1000–3000 Hz.— It may be debated whether the initial degradation characterized by a frequency of 1000–3000 Hz is related to the Ni/YSZ or LSM/YSZ electrode. Based on the characteristic frequency, the minor initial degradation may be assigned to a degradation of the LSM/YSZ electrode.[64] However, the contribution from the Ni/YSZ was observed as low as 2000 Hz.[39] Further, the initial degradation of the Ni/YSZ electrode (mainly characterized 100–200 Hz) shifted down from just below 1000 Hz to the 100–200 Hz (see above and Fig. 4 and 5). This means that at low degradation, the degradation related to the Ni/YSZ electrode may be observed at ~1000 to 2000 Hz, and the minor initial degradation may therefore be assigned to a degradation of the Ni/YSZ electrode.

Regardless of the electrode assignment, it seems that the initial degradation may be affected by the current density (higher initial degradation when operating at -0.50 A/cm^2 compared to when operating at -0.25 A/cm^2, Fig. 2 and 7A).

Assuming that the degradation is related to the LSM/YSZ electrode, from Fig. 7A and 8, it seems like the minor initial degradation is reversible (passivation) when pure oxygen is supplied to the electrode. Because this passivation/activation phenomenon of the LSM/YSZ electrode occurred only when supplying oxygen to the electrode, it may be speculated to be caused by altered oxygen stoichiometry (as a consequence of pO_2) or cation diffusivity (as a consequence of the applied current, see above) in the active electrode.

Assuming that the degradation is related to the Ni/YSZ electrode, from Fig. 7A and 8, it seems like the minor initial degradation is reversible (passivation), similar to the kinetics observed during formation of volatile scales.[72,73] Formation of such volatile impurity phases may originate from impurities in the raw materials such as silica and sodium. In this case, the degradation is caused by impurities in the raw materials migrating to the surface and the TPB. Hereafter, the impurities are at least partly removed from TPB by the gas stream resulting in the long-term activation observed when applying cleaned inlet gases. The cause of the in-plane voltage as shown in Fig. 7B suggests that the activation is caused by removing impurities from the raw materials.

In summary, the degradation in the performance of SOECs is heavily influenced by the adsorption of impurities at the TPB in the Ni/YSZ electrode during electrolysis. Adsorption of impurities at the TPB inevitably causes an increased polarization resistance due to a partial blockage of the TPB. Because in addition to surface diffusion of oxygen, diffusion of protons through Ni and YSZ may also be involved in the reaction mechanism for H_2O/H_2 reduction/oxidation, reactions involving H_2O/H_2 may be less sensitive to the blockage of the TPB by impurities than reactions involving CO_2/CO where no proton diffusion is involved in the reaction, thus explaining the relatively higher degradation by impurities observed during CO_2 electrolysis. The passivation/degradation at the Ni/YSZ electrode, which is characterized by a frequency of ~100 to 200 Hz, can be eliminated by cleaning the inlet gases to the Ni/YSZ electrode. Cleaning the inlet gases resulted in cell operation without any long-term degradation.

Conclusion

Degradation of Ni/YSZ-based SOECs, when applied for H_2O electrolysis, CO_2 electrolysis, and co-electrolysis of H_2O and CO_2, was examined. Several long-term durability tests at 850°C and -0.25 to -0.5 A/cm^2 were performed. When applying the gases as received, the cells passivated/degraded with a rate between 0.45 and 0.70 mV/h over the first few hundred hours and a long-term degradation between 0.003 and 0.032 mV/h, regardless of the electrolysis conditions. However, when applying clean inlet gases, no degradation was observed; in fact some cells activate slightly. The durability of these SOECs are heavily influenced by impurities in the inlet gases.

When operating the cells at current densities up to at least -0.5 A/cm^2, only polarization degradation is observed and no ohmic degradation. The polarization degradation can be divided into two degradation mechanisms, one at the Ni/YSZ electrode (with a characteristic frequency of 100–200 Hz in the impedance spectra), which is heavily influenced by impurities and one minor initial degradation occurring either at the Ni/YSZ or LSM/YSZ electrodes (with a characteristic frequency of ~1000 to 3000 Hz). The long-term activation of the cells when introducing steam may be caused by the removal of impurities from the cell (raw material).

The degradation occurring at the Ni/YSZ (with a characteristic frequency of 100–200 Hz) electrode can be completely eliminated by cleaning the inlet gas to the electrode, whereas the degradation at the LSM/YSZ electrode is not affected by cleaning the inlet gas. The degradation of these SOECs is thereby caused by the adsorption of impurities, and cleaning the inlet gases to the Ni/YSZ electrode may be a solution for operating these Ni/YSZ-based SOECs without any long-term degradation.

Acknowledgments

This work was financially supported by The Danish National Advanced Technology Foundations advanced technology platform "Development of 2nd Generation Bioethanol Process and Technology" and the Danish Council for Strategic Research, via the Strategic Electrochemistry Research Center (SERC, www.serc.dk).

The Technical University of Denmark assisted in meeting the publication costs of this article.

References

1. A. D. Ebner and J. A. Ritter, *Sep. Sci. Technol.*, **44**, 1273 (2009).
2. H. Chalmers, M. Lucquiaud, J. Gibbins, and M. Leach, *J. Environ. Eng.*, **135**, 449 (2009).
3. J. K. Stolaroff, D. W. Keith, and G. V. Lowry, *Environ. Sci. Technol.*, **42**, 2728 (2008).
4. F. Zeman, *Environ. Sci. Technol.*, **41**, 7558 (2007).
5. K. S. Lackner, H. J. Ziock, and P. Grimes, in Proceedings of the 24th International Technical Conference on Coal Utilization and Fuel Systems, Clearwater, Florida, B. Sakkestad, ed., p. 885 (1999).
6. S. Elliott, K. S. Lackner, H. J. Ziock, M. K. Dubey, H. P. Hanson, S. Barr, N. A. Ciszkowski, and D. R. Blake, *Geophys. Res. Lett.*, **28**, 1235 (2001).
7. K. S. Lackner, *Science*, **300**, 1677 (2003).
8. K. S. Lackner, *The Physics Perspective on Energy Supply and Climate Change: A Critical Assessment*, Springer Verlag, Bad Honnef (2009).
9. S. D. Ebbesen and M. Mogensen, *Electrochem. Solid-State Lett.*, **13**(9), B106 (2010).
10. C. Graves, S. D. Ebbesen, M. Mogensen, and K. S. Lackner, *Renewable Sustainable Energy Rev.*, Accepted.
11. S. H. Jensen, P. H. Larsen, and M. Mogensen, *Int. J. Hydrogen Energy*, **32**, 3253 (2007).
12. M. A. Liepa and A. Borhan, *Int. J. Hydrogen Energy*, **11**, 435 (1986).
13. M. Ni, M. K. H. Leung, and D. C. Leung, *Int. J. Hydrogen Energy*, **32**, 4648 (2007).
14. J. Sigurvinsson, C. Mansilla, P. Lovera, and F. Werkoff, *Int. J. Hydrogen Energy*, **32**, 1174 (2007).

15. S. D. Ebbesen, C. Graves, and M. Mogensen, *Int. J. Green Energy*, **6**, 646 (2009).
16. W. Doenitz, R. Schmidberger, E. Steinheil, and R. Streicher, *Int. J. Hydrogen Energy*, **5**, 55 (1980).
17. A. O. Isenberg, *Solid State Ionics*, **3–4**, 431 (1981).
18. *Electrochemical Hydrogen Technologies: Electrochemical Production and Combustion of Hydrogen*, H. Wendt, Editor, Elsevier, Amsterdam, The Netherlands (1990).
19. A. Hauch, S. D. Ebbesen, S. H. Jensen, and M. Mogensen, *J. Mater. Chem.*, **18**, 2331 (2008).
20. O. A. Marina, L. R. Pederson, M. C. Williams, G. W. Coffey, K. D. Meinhardt, C. D. Nguyen, and E. C. Thomsen, *J. Electrochem. Soc.*, **154**, B452 (2007).
21. K. R. Sridhar, *J. Br. Interplanet. Soc.*, **49**, 435 (1996).
22. K. R. Sridhar and B. T. Vaniman, *Solid State Ionics*, **93**, 321 (1997).
23. S. D. Ebbesen and M. Mogensen, in Proceedings of the 32nd International Conference & Exposition on Advanced Ceramics and Composites, The American Ceramic Society, p. 271 (2008).
24. S. D. Ebbesen and M. Mogensen, *J. Power Sources*, **193**, 349 (2009).
25. G. Tao, K. R. Sridhar, and C. L. Chan, *Solid State Ionics*, **175**, 621 (2004).
26. F. Bidrawn, G. Kim, G. Corre, J. T. S. Irvine, J. M. Vohs, and R. J. Gorte, *Electrochem. Solid-State Lett.*, **11**, B167 (2008).
27. R. D. Green, C. C. Liu, and S. B. Adler, *Solid State Ionics*, **179**, 647 (2008).
28. J. M. Wei and E. Iglesia, *J. Catal.*, **224**, 370 (2004).
29. L. Elikan, J. P. Morris, and C. K. Wu, NASA Report CR-2014, NASA Research Center (1972).
30. A. O. Isenberg and C. E. Verostko, Carbon Dioxide and Water Vapor High Temperature Electrolysis, SAE Technical Paper Series No. 891506, in The Nineteenth Intersociety Conference on Environmental Systems, San Diego, CA, July 24–26, (1989).
31. C. M. Stoots, J. E. O'Brien, J. S. Herring, and J. J. Hartvigsen, *J. Fuel Cell Sci. Technol.*, **6**, 011014 (2009).
32. Z. Zhan, W. Kobsiriphat, J. R. Wilson, M. Pillai, I. Kim, and S. A. Barnett, *Energy Fuels*, **23**, 3089 (2009).
33. J. Hartvigsen, S. Elangovan, J. O'Brien, C. Stoots, and J. Herring, *ECS Trans.*, **7**(1), 357 (2007).
34. J. Schefold, A. Brisse, and M. Zahid, *J. Electrochem. Soc.*, **156**, B897 (2009).
35. A. Brisse, J. Schefold, and M. Zahid, *Int. J. Hydrogen Energy*, **33**, 5375 (2008).
36. W. Dönitz, E. Erdle, and R. Streicher, *Electrochemical Hydrogen Technologies: Electrochemical Production and Combustion of Hydrogen*, p. 219, Elsevier, Amsterdam, The Netherlands (1990).
37. S. D. Ebbesen, J. Høgh, and M. Mogensen, Production of Hydrogen and Synthesis Gas by High Temperature Electrolysis, in Proceedings of Risø International Energy Conference 2009, Risø National Laboratory for Sustainable Energy, p. 162 (2009).
38. A. Hauch, S. H. Jensen, S. Ramousse, and M. Mogensen, *J. Electrochem. Soc.*, **153**, A1741 (2006).
39. A. Hauch, Ph.D. Thesis, Risø National Laboratory, Roskilde, Denmark (2007).
40. A. Hauch, S. H. Jensen, J. B. Bilde-Sørensen, and M. Mogensen, *J. Electrochem. Soc.*, **154**, A619 (2007).
41. A. Hauch, S. D. Ebbesen, S. H. Jensen, and M. Mogensen, *J. Electrochem. Soc.*, **155**, B1184 (2008).
42. S. H. Jensen, Ph.D. Thesis, Risø National Laboratory, Roskilde, Denmark (2006).
43. S. H. Jensen, A. Hauch, P. V. Hendriksen, and M. Mogensen, *J. Electrochem. Soc.*, **156**, B757 (2009).
44. J. E. O'Brien, C. M. Stoots, J. S. Herring, and J. J. Hartvigsen, *Nucl. Technol.*, **158**, 118 (2007).
45. A. Hagen, R. Barfod, P. V. Hendriksen, Y. L. Liu, and S. Ramousse, *J. Electrochem. Soc.*, **153**, A1165 (2006).
46. S. H. Jensen, A. Hauch, P. V. Hendriksen, M. Mogensen, N. Bonanos, and T. Jacobsen, *J. Electrochem. Soc.*, **154**, B1325 (2007).
47. M. Y. Gong, X. B. Liu, J. Trembly, and C. Johnson, *J. Power Sources*, **168**, 289 (2007).
48. K. V. Hansen, K. Norrman, and M. Mogensen, *J. Electrochem. Soc.*, **151**, A1436 (2004).
49. A. Hauch, J. R. Bowen, L. T. Kuhn, and M. Mogensen, *Electrochem. Solid-State Lett.*, **11**, B38 (2008).
50. A. E. Hughes and S. P. S. Badwal, *Solid State Ionics*, **46**, 265 (1991).
51. J. Høgh, Ph.D. Thesis, Risø National Laboratory, Roskilde, Denmark (2005).
52. K. V. Jensen, Ph.D. Thesis, Risø National Laboratory, Roskilde, Denmark (2002).
53. K. V. Jensen, R. Wallenberg, I. Khorkendorff, and M. Mogensen, *Solid State Ionics*, **160**, 27 (2003).
54. Y. L. Liu, S. Primdahl, and M. Mogensen, *Solid State Ionics*, **161**, 1 (2003).
55. Y. L. Liu and C. G. Jiao, *Solid State Ionics*, **176**, 435 (2005).
56. Y. Matsuzaki and I. Yasuda, *Solid State Ionics*, **132**, 261 (2000).
57. M. Mogensen, K. V. Jensen, M. J. Jørgensen, and S. Primdahl, *Solid State Ionics*, **150**, 123 (2002).
58. J. F. B. Rasmussen and A. Hagen, *J. Power Sources*, **191**, 534 (2009).
59. H. Yokokawa, T. Watanabe, A. Ueno, and K. Hoshino, *ECS Trans.*, **7**(1), 133 (2007).
60. P. H. Larsen, C. Bagger, S. Linderoth, M. Mogensen, S. Primdahl, M. J. Jørgensen, P. V. Hendriksen, B. Kindl, N. Bonanos, F. W. Poulsen, et al., in Proceedings of Solid Oxide Fuel Cell VII (SOFC VII), The Electrochemical Society, p. 28 (2001).
61. M. J. Jørgensen and M. Mogensen, *J. Electrochem. Soc.*, **148**, A433 (2001).
62. M. Mogensen and P. V. Hendriksen, *High Temperature Solid Oxide Fuel Cells: Fundamentals, Design, and Applications*, p. 261, Elsevier, London (2003).
63. S. D. Ebbesen and M. Mogensen, Pat. appl. EP69427 (2010).
64. R. Barfod, M. Mogensen, T. Klemenso, A. Hagen, Y. L. Liu, and P. V. Hendriksen, *J. Electrochem. Soc.*, **154**, B371 (2007).
65. T. Jacobsen, P. V. Hendriksen, and S. Koch, *Electrochim. Acta*, **53**, 7500 (2008).
66. S. Primdahl and M. Mogensen, *J. Electrochem. Soc.*, **146**, 2827 (1999).
67. S. Primdahl and M. Mogensen, *J. Electrochem. Soc.*, **145**, 2431 (1998).
68. A. Hagen, M. Menon, R. Barfod, P. V. Hendriksen, S. Ramousse, and P. H. Larsen, *Fuel Cells*, **6**, 146 (2006).
69. C. W. Bale, P. Chartrand, S. A. Degterov, G. Eriksson, K. Hack, R. Ben Mahfoud, J. Melançon, A. D. Pelton, and S. Petersen, FactSage Thermochemical Software and Databases, Center for Research in Computational Thermochemistry École Polytechnique (Université de Montréal), Montréal, Québec, Canada and GTT-Technologies, 52134 Herzogenrath, Germany (2002).
70. R. Knibbe, M. L. Traulsen, A. Hauch, S. D. Ebbesen, and M. Mogensen, *J. Electrochem. Soc.*, **157**, B1209 (2010).
71. A. Hagen, Fuel Cells and Solid State Chemistry Division, Risø National Laboratory for Sustainable Energy, The Technical University of Denmark, Personal communication (2009).
72. E. J. Opila and R. E. Hann, *J. Am. Ceram. Soc.*, **80**, 197 (1997).
73. D. Wajszel, *J. Electrochem. Soc.*, **110**, 504 (1963).